Bioorganic Chemistry 112 (2021) 104968

Contents lists available at ScienceDirect

Bioorganic Chemistry

journal homepage: www.elsevier.com/locate/bioorg

Design and synthesis of novel substituted benzyl pyrrolopyrimidine derivatives as selective BTK inhibitors for treating mantle cell lymphoma

Fansheng Ran [a,c], Yang Liu [b], Xin Chen [a], Huijun Zhuo [a], Changqing Xu [a], Yuxia Li [a], Xiaoming Duan [a], Guisen Zhao [a,*]

[a] Department of Medicinal Chemistry, Key Laboratory of Chemical Biology (Ministry of Education), School of Pharmaceutical Sciences, Cheeloo College of Medicine, Shandong University, Jinan 250012, Shandong, PR China
[b] Department of Lymphoma and Myeloma, The University of Texas MD Anderson Cancer Center, Houston, TX 77030, USA
[c] School of Pharmacy and Jiangsu Province Key Laboratory for Inflammation and Molecular Drug Target, Nantong University, Nantong 226001, PR China

ARTICLE INFO

Keywords:
Mantle cell lymphoma
BTK inhibitor
Apoptosis
Antitumor
Selectivity

ABSTRACT

Ibrutinib, a potent irreversible Bruton's tyrosine kinase (BTK) inhibitor, was approved by the FDA for treating mantle cell lymphoma (MCL). Although ibrutinib exhibited excellent antitumor activity, it was associated with certain adverse reactions, with off-target effects against EGFR, Itk and Src family kinases. Our studies yielded a novel series of substituted benzyl pyrrolopyrimidine derivatives capable of potent inhibition of BTK. Compared with ibrutinib, compound **15c** exhibited potent BTK inhibitory activity and enhanced antiproliferative activity, a 12–24-fold increase, against MCL cell lines, with IC_{50} values lower than 1 μM. Low micromolar doses of **15c** inhibited the BCR signaling pathway and strongly induced the apoptosis of Z138 cells. Ibrutinib and **15c** induced autophagy in a dose-dependent manner in Z138 cells. Moreover, compound **15c** induced the production of reactive oxygen species (ROS), which may be a reason for its potent antiproliferative activity. Importantly, compound **15c** showed greater BTK selectivity than ibrutinib, indicating a potentially safer treatment of MCL.

1. Introduction

Mantle cell lymphoma (MCL), a type of non-Hodgkin lymphoma, is characterized by involvement of the lymph nodes, blood, bone marrow and spleen. The remission duration of standard therapies against MCL is short, and the median overall survival (OS) is 4–5 years [1]. The molecular hallmark of MCL is chromosomal translocation t(11;14)(q13;q32), leading to the overexpression of cyclin D1 [2]. The B-cell receptor (BCR) signaling pathway plays a key role in the development of B-cell malignancies. Constitutive or aberrant activation of the BCR signaling cascade has been implicated in the proliferation, survival, differentiation, maturation, and apoptosis of B-cell malignancies [3].

Bruton tyrosine kinase (BTK), a cytoplasmic protein tyrosine kinase, was initially implicated in the pathogenesis of X-linked agammaglobulinemia [4]. The BTK gene, which is located on the X chromosome in the region Xq21.3-22.1, was isolated and identified in 1993 [5]. BTK, with 659 amino acid residues, is expressed in all hematopoietic lineage cells except for T cells [6]. BTK is a key effector of the BCR signaling pathway and plays significant roles in the initiation and progression of B-cell malignancies. BTK is activated by upstream Src family kinases and then phosphorylates downstream phospholipase-Cγ2 (PLCγ2), leading to Ca^{2+} mobilization and activation of the NF-κB and MAP kinase pathways [4]. These proximal signaling events facilitate the expression of genes related to cell survival and proliferation. BTK is commonly overexpressed in MCL. In recent years, BTK inhibitors have been investigated as potential treatments for MCL.

In 2013, ibrutinib (**1**), a first-generation irreversible BTK inhibitor, was approved by the FDA to treat MCL, chronic lymphocytic leukemia (CLL), Waldenström's macroglobulinemia (WM) and chronic graft-versus-host disease (cGVHD) [7–10]. However, side effects, including rash, diarrhea, bleeding and atrial fibrillation, have been reported, and these are believed to be associated with off-target effects on EGFR and SRC family proteins [5,11]. Nearly 30% of patients receiving ibrutinib therapy ultimately discontinue treatment due to related adverse events, highlighting the importance of developing more-selective BTK inhibitors [12].

Several other BTK inhibitors have also made breakthroughs in clinical studies. Acalabrutinib (**2**) and zanubrutinib (**3**), second-generation

* Corresponding author.
E-mail address: guisenzhao@sdu.edu.cn (G. Zhao).

https://doi.org/10.1016/j.bioorg.2021.104968
Received 26 January 2021; Received in revised form 19 April 2021; Accepted 4 May 2021
Available online 7 May 2021

BTK inhibitors, were approved by the FDA for the treatment of MCL in 2017 and 2019, respectively [13–15]. Recently, orelabrutinib (**4**) was approved by CFDA for the treatment of MCL and CLL/SLL [16]. Moreover, a considerable number of clinical studies of BTK inhibitors, including tirabrutinib (**5**, phase 2) and evobrutinib (**6**, phase 3), are ongoing (Fig. 1**A**) [17,18].

It has been reported that the pharmacophore model of BTK inhibitors consists of large hydrophobic groups, aromatic heterocyclic nuclei, linkers, and warheads or terminal groups. The aromatic core structure with a hydrogen bond donor and acceptor occupies the hinge region of BTK. A large hydrophobic group extending to the hydrophobic pockets adjacent to the hinge region mediates hydrophobic interactions. The linker connects the warhead or terminal group extending to Cys481 or the solvent region in the enzyme (Fig. 1**B**) [14,19–22]. The 4-phenoxyphenyl group and pyridine-2-benzamide group are common hydrophobic groups in reported BTK inhibitors. In our previous study, we found that compound **7** with a benzyl linker showed moderate BTK inhibitory activity (IC_{50} = 229 nM) [22]. In this work, we made additional structural modifications to compound **7**. Specifically, we retained the backbone of lead compound **7**, replaced the 4-phenoxyphenyl hydrophobic group with a pyridine-2-benzamide group, and introduced different terminal groups or warheads on the benzyl linker to produce reversible or irreversible BTK inhibitors for further evaluation of the structure–activity relationship. Herein, a series of substituted benzyl pyrrolopyrimidine derivatives are reported as novel potent BTK inhibitors (Fig. 1**C**).

2. Results and discussion

2.1. Chemistry

The synthetic routes for these compounds are illustrated in Scheme 1. Condensation of various substituted 2-aminopyridine (**8**) and 4-bromobenzoic acid afforded compound **9**. Subsequent coupling of compound **9** with bis(pinacolato)diboron catalyzed by palladium acetate produced compound **10**. Compound **11** reacted with various substituted benzyl bromides to give compound **12**, which reacted with compound **10** via a Suzuki reaction to provide target compound **13**. Reduction of the nitro groups on compound **13** in the presence of Fe-NH_4Cl yielded compound **14**. Following condensation of compounds **14** and acryloyl chloride or chloroacetyl chloride afforded the final product, compound **15**.

2.2. BTK inhibitory activity

The newly synthesized compounds were evaluated for their activity against BTK using a kinase profiler radiometric protein kinase assay. The initial screening was performed at a concentration of 1 μM for each compound. Compounds exhibiting BTK inhibition rates ≥ 80% at 1 μM were selected for determination of IC_{50} values. As shown in Table 1, most compounds exhibited moderate BTK inhibitory activity at 1 μM. Compared with chlorine and bromine substituents, the fluorine substituent exhibited the best BTK inhibitory activity (**13a** *vs* **13b** & **13c**, **13g** *vs* **13h** & **13i**, **13m** *vs* **13n** & **13o**). When the R groups were Br, Cl, NO_2, or NH_2, introduction of a trifluoromethyl group at the R_1 position produced an obvious improvement in BTK inhibition compared to the introduction of a methyl group and hydrogen (**13o** *vs* **13i** & **13c**, **13n** *vs* **13h** & **13b**, **13q** *vs* **13k** & **13e**, **14i** *vs* **14f** & **14c**). Analyzing compounds **14g**, **14h** and **14i**, we found that amino substituents at the *para*-position produced more-potent BTK inhibitory activity than those at the *meta*-position or *ortho*-position (**14i** $IC_{50} = 47 \pm 5$ nM, **14 h** $IC_{50} = 87 \pm 9$ nM, **14g** $IC_{50} = 296 \pm 11$ nM). Compared to **15b** and **15d** with a acrylamide group, **15a** and **15c** with a chloroacetamide group exhibited greater efficacy against BTK, which was consistent with previously reported findings [22]. Among these new compounds, **15c**, an irreversible inhibitor, showed the highest BTK inhibitory activity.

2.3. Antiproliferative activity against MCL cell lines

We selected potent BTK inhibitors (IC_{50} < 100 nM) to investigate

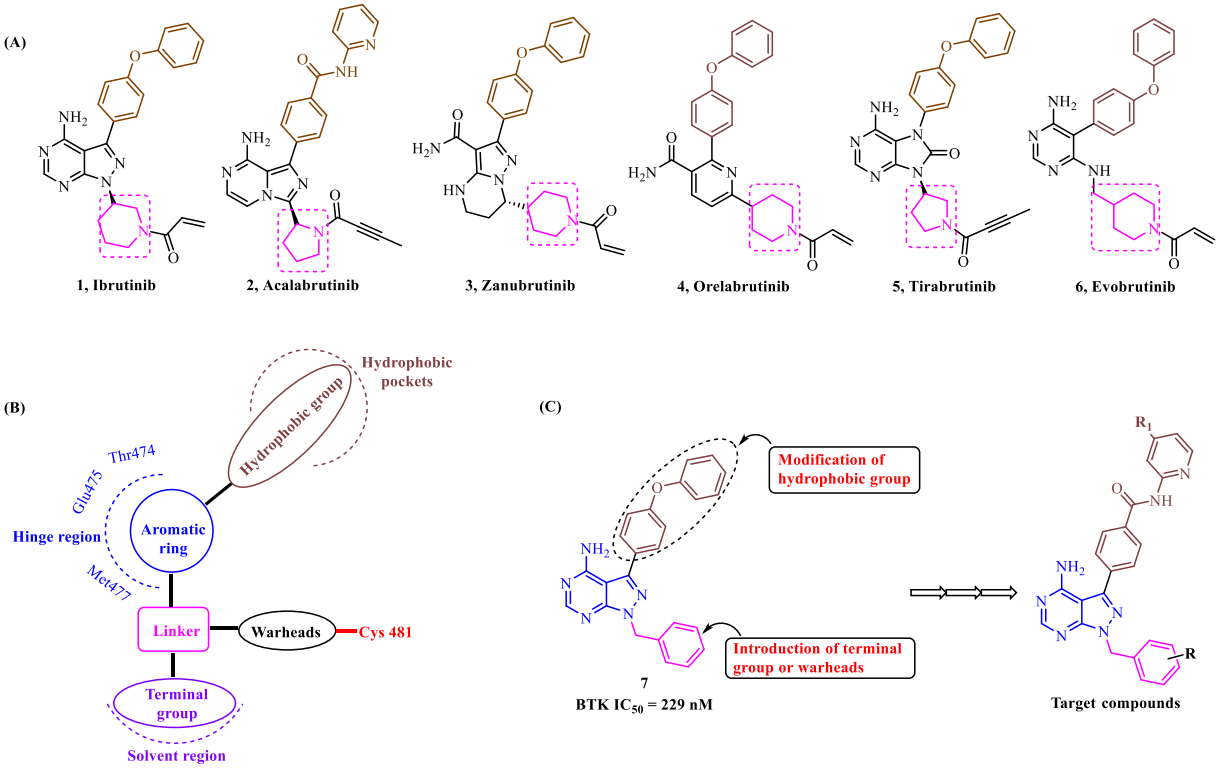

Fig. 1. (**A**) Representative chemical structures of the novel BTK inhibitors; (**B**) Common features of BTK inhibitors; (**C**) Design of target compounds.

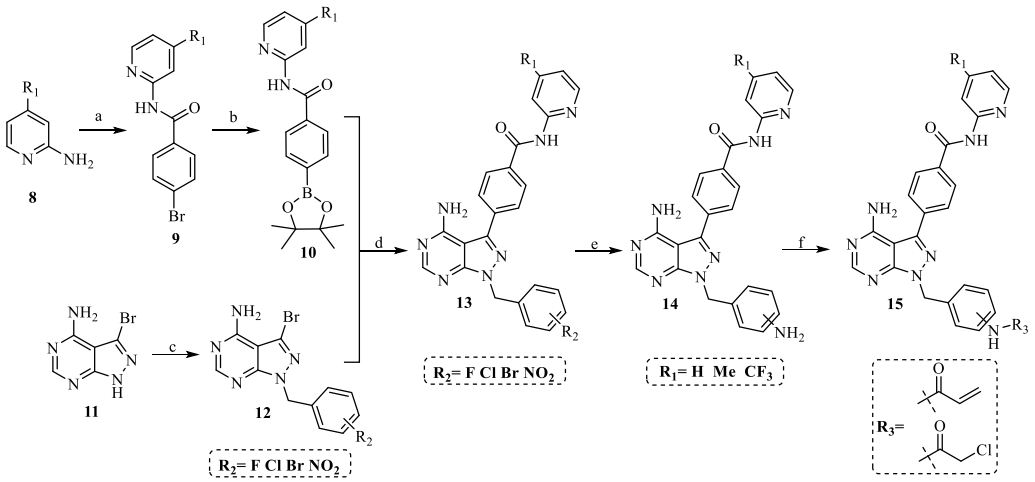

Scheme 1. Synthetic routes of compounds **13**, **14** and **15**. Reagents and conditions: (a) 4-bromobenzoic acid, HBTU, Et_3N, DMF, r.t., 12 h; (b) $Pd(OAc)_2$, X-PHOS, KOAc, bis(pinacolato)diboron, 1,4-dioxane, 90 °C, 12 h; (c) substituted benzyl bromide, K_2CO_3, DMF, r.t., 5 h; (d) $Pd(PPh_3)_4$, K_3PO_4, 1,4-dioxane/H_2O = 4/1, 120 °C, 24 h; (e) Fe, NH_4Cl, EtOH/H_2O = 3/1, 90 °C, 6 h; (f) acryloyl chloride or chloroacetyl chloride, Et_3N, THF, 0 °C to r.t., 5 h.

Table 1
The inhibitory effects of series **13**, **14** and **15** on BTK activity.

Code	R_1	R	BTK inhibition (%) at 1 μM	BTK IC_{50} (nM)[a]	Code	R_1	R	BTK inhibition (%) at 1 μM	BTK IC_{50} (nM)[a]
Ibrutinib	–	–	101	8 ± 0.6	**13p**	CF_3	2-NO_2	91	127 ± 10
13a	H	2-F	67	ND[b]	**13q**	CF_3	3-NO_2	80	444 ± 18
13b	H	2-Cl	56	ND[b]	**13r**	CF_3	4-NO_2	65	ND[b]
13c	H	2-Br	53	ND[b]	**14a**	H	2-NH_2	44	ND[b]
13d	H	2-NO_2	49	ND[b]	**14b**	H	3-NH_2	29	ND[b]
13e	H	3-NO_2	8	ND[b]	**14c**	H	4-NH_2	64	ND[b]
13f	H	4-NO_2	32	ND[b]	**14d**	Me	2-NH_2	63	ND[b]
13g	Me	2-F	87	109 ± 8	**14e**	Me	3-NH_2	71	ND[b]
13h	Me	2-Cl	75	ND[b]	**14f**	Me	4-NH_2	71	ND[b]
13i	Me	2-Br	72	ND[b]	**14g**	CF_3	2-NH_2	81	296 ± 11
13j	Me	2-NO_2	76	ND[b]	**14h**	CF_3	3-NH_2	95	87 ± 9
13k	Me	3-NO_2	26	ND[b]	**14i**	CF_3	4-NH_2	98	47 ± 5
13l	Me	4-NO_2	48	ND[b]	**15a**	CF_3	3-$NHCOCH_2Cl$	99	52 ± 3
13m	CF_3	2-F	90	146 ± 5	**15b**	CF_3	3-$NHCOCHCH_2$	47	ND[b]
13n	CF_3	2-Cl	81	217 ± 9	**15c**	CF_3	4-$NHCOCH_2Cl$	100	45 ± 1
13o	CF_3	2-Br	82	200 ± 7	**15d**	CF_3	4-$NHCOCHCH_2$	75	ND[b]

[a] All IC_{50} values were obtained by testing in triplicate ND[b] = Not detected

their antiproliferative activity against four MCL cell lines using a Cell Titer-Glo luminescent cell viability assay. As illustrated in Table 2, compared with ibrutinib, amino-substituted compounds **14h** and **14i** exhibited poor antiproliferative activity in MCL cells, whereas compounds **15a** and **15c** demonstrated excellent antiproliferative activity in MCL cell lines. Compound **15c** was the most potent antitumor agent of MCL cells, with IC_{50} values lower than 1 μM, which was 12–24-fold lower than ibrutinib.

2.4. Inhibitory effects on BTK signaling

To further evaluate the inhibitory effects of **15c** on BTK signaling, immunoblotting was performed to assess the phosphorylation of BTK and its downstream effector PLCγ2 in Z138 cells. As shown in Fig. 2**A**, after 24 h of treatment with **15c**, phosphorylation of BTK and PLCγ2 was significantly inhibited, suggesting that **15c** strongly inhibits the BTK signaling pathway.

Table 2
Cell proliferation assay assessing the effects of target compounds on MCL cell lines.[a]

Code	Cell viability assay, IC_{50} (μM)[a]			
	Rec-1	Mino	Maver-1	Z138
Ibrutinib	8.6 ± 1.2	4.9 ± 0.8	6.6 ± 0.6	9.7 ± 0.5
14 h	45.2 ± 5.8	34.7 ± 2.2	>60	>60
14i	8.6 ± 0.9	16.3 ± 1.7	>60	40.5 ± 6.1
15a	1.0 ± 0.08	0.4 ± 0.06	0.4 ± 0.03	0.8 ± 0.04
15c	0.7 ± 0.05	0.4 ± 0.02	0.4 ± 0.01	0.4 ± 0.01

[a] All IC_{50} values were obtained by testing in triplicate.

2.5. Cell apoptosis assay

We continued to test the effects of **15c** on the apoptosis of Z138 cells using the annexin V-FITC/propidium iodide (PI) binding assay. As illustrated in Fig. 2**B**, compound **15c** demonstrated strong apoptosis induction of Z138 cells in a dose-dependent manner. Treating Z138 cells with 1 μM **15c** for 24 h resulted in the apoptosis of more than 95% of the cells.

2.6. Inducing autophagy in MCL cells

Autophagy is considered a mechanism of cell death induced by death programs. Muqbil et al. reported that ibrutinib treatment caused autophagic cell death of Hodgkin's lymphoma cells [23]. In another study, Wang et al. showed that the antitumor mechanism of ibrutinib involves the activation of autophagy pathways in a glioblastoma model [24]. We therefore investigated the induction of autophagy by ibrutinib and **15c** in Z138 cells. As shown in Fig. 2**C**, the Western blotting results showed

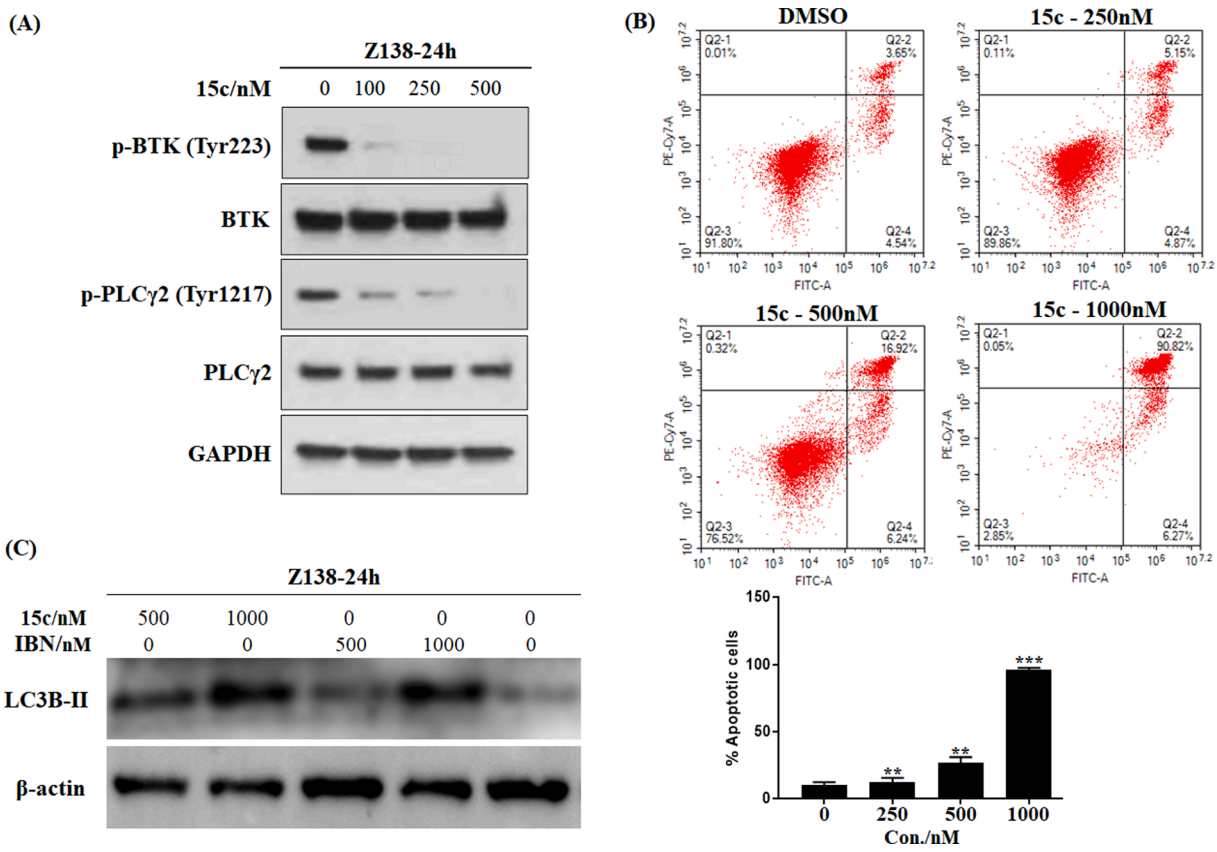

Fig. 2. **(A)** Effect of **15c** on BTK signaling in Z138 cells after 24 h of treatment. (**B**) Apoptosis assay with **15c** at the indicated concentrations in Z138 cells treated for 24 h. (**C**) Autophagy induction by **15c** and ibrutinib in Z138 cells. Western blotting results showing expression of LC3B-II and β-actin in Z138 cells treated with different concentrations of **15c** and ibrutinib. Significance is indicated as *P < 0.05, **P < 0.01, and ***P < 0.001 compared with the DMSO control.

that expression of LC3B-II, a critical component in regulating the formation of autophagosomes, significantly increased in a dose-dependent manner after ibrutinib and **15c** treatment of Z138 cells.

2.7. Regulation of reactive oxygen species levels

Reactive oxygen species (ROS) play important roles in the genesis, progression, and metastasis of tumors. The proliferation, angiogenesis,

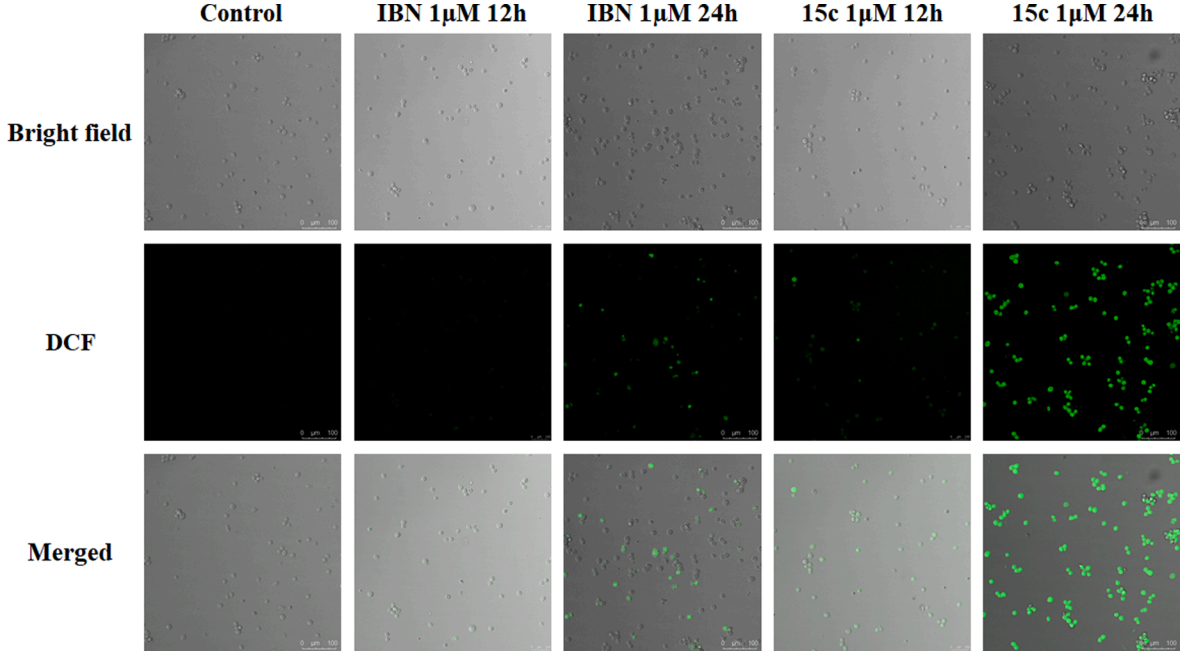

Fig. 3. ROS levels in Z138 cells after 12 h or 24 h of treatment with 1 μM ibrutinib or **15c**. The DCFH-DA probe is hydrolyzed to DCFH in cells, which reacts with ROS, generating DCF with green fluorescence. The intensity of the green fluorescence reflects the level of ROS.

and metastasis of cancer cells are promoted under low levels of oxidative stress. However, high levels of ROS can cause irreversible damage to lipids and DNA, ultimately resulting in the apoptosis of cancer cells [25]. It has been reported that BTK negatively regulates the production of ROS and stimulation-induced apoptosis in human neutrophils [26]. Galicia-Vazquez et al. found that ibrutinib enhanced ROS levels in CLL [27]. We evaluated the effect of ibrutinib and **15c** on ROS levels in MCL via a DCFH-DA probe. As demonstrated in Fig. 3, ibrutinib and **15c** enhanced ROS production in Z138 cells in a time-dependent manner. Compared with the ibrutinib groups, the **15c** groups showed higher ROS levels at low micromolar concentrations, which may be a reason for their higher antiproliferative activity.

2.8. Selectivity compared with other kinases

We further tested the kinase selectivity of **15c** against a panel of 20 kinases. As shown in Table 3, ibrutinib exhibited potent inhibitory activity against 19 kinases, showing poor selectivity. Compound **15c** exhibited no inhibitory activity against 16 kinases, including EGFR, Itk, and Src family kinases. Ibrutinib, which inhibits EGFR and Src family kinases, can induce gastrointestinal adverse effects, dramatic cutaneous toxicity and high bleeding risk [11]. Moreover, ibrutinib inhibited Itk in NK cells, which could reduce the effect of rituximab-induced antibody-dependent cell-mediated cytotoxicity (ADCC), which would be a potential drawback in combination regimens [28–29]. Compound **15c** exhibited greater BTK selectivity than ibrutinib and had the potential for better safety in the treatment of MCL.

2.9. Molecular modeling

The binding mode of compound **15c** with BTK (PDB ID: 5fbo) as determined by molecular docking analysis is shown in Fig. 4. The pyrazolopyrimidine core occupies the hinge region, forming several important hydrogen bonds with Glu475 and Met477. The hydrophobic group extends to the hydrophobic pocket behind the gatekeeper, Thr474, forming an edge-to-face aromatic interaction with Phe540. Furthermore, the acylamide in the hydrophobic group forms a hydrogen bond with the carbonyl of Ser538, which may be the essential interaction for the kinase selectivity of **15c**.

3. Conclusion

In this study, we described the design, synthesis and results of biological evaluations of novel substituted benzyl pyrrolopyrimidine derivatives as potential agents for treating MCL. Among these compounds, **15c** showed potent BTK inhibitory activity and high enzyme selectivity. In kinase screening with a panel of 20 kinases, **15c** demonstrated a promising selectivity profile toward 16 kinases. Compound **15c** induced a high apoptosis rate of Z138 cells in a dose-dependent manner at low micromolar concentrations. Compound **15c** also enhanced ROS production in Z138 cells in a time-dependent manner. Compared with ibrutinib, **15c** exerted 12- to 24-fold improvement in antiproliferative activity against MCL cell lines, with IC_{50} values lower than 1 μM, supporting further evaluation and development of the promising candidate **15c** in cancer therapy.

Table 3
Inhibition efficacy (%) among different kinases at 1 μM by **15c** and ibrutinib.

Kinases	15c	Ibrutinib	Kinases	15c	Ibrutinib
Blk	98	100	**Itk**	29	86
Bmx	94	102	**Jak3**	48	54
Brk	37	92	**Lck**	32	99
Csk	−9	87	**Lyn**	8	99
EGFR	26	98	**Ptk5**	16	91
ErbB2	37	73	**Src**	12	96
ErbB4	72	101	**Srm**	27	100
Fgr	13	92	**Tec**	84	103
Fyn	20	97	**Txk**	85	97
Hck	−4	96	**Yes**	8	102

4. Experimental section

4.1. Chemistry

All chemical reagents and solvents were purchased from commercial sources and used without further purification. Reactions were monitored using thin-layer chromatography (TLC) performed on SGF254 plates. Column chromatography was carried out with the indicated solvents using silica gel (60 Å, 200–300 mesh). Melting points were determined using a Büchi capillary melting point apparatus (Buchi Labortechnik AG, Switzerland) without correction. Using tetramethylsilane (TMS) as an internal standard in DMSO-d_6 or $CDCl_3$, NMR spectra were recorded at 400 MHz for ^1H and 100 MHz for ^{13}C on a Bruker Avance DRX-400 spectrometer (Bruker, Germany). The chemical shifts (δ) are reported in parts per million (ppm) using tetramethylsilane as an internal standard.

4.2. General synthesis of compounds

4.2.1. Preparation of compound *9*

A mixture of 4-bromobenzoic acid (10 mmol), HBTU (12 mmol) and triethylamine (30 mmol) in DMF (30 mL) was stirred under ice-cold conditions for 30 min. Then, compound **8** (10 mmol) was added, and the mixture was stirred at room temperature for 12 h. Upon completion, the reaction solution was poured into water (300 mL), and the suspension was filtered to give compound **9**.

4.2.2. Preparation of compound *10*

A premixed and degassed solution of $Pd(OAc)_2$ (0.23 mmol) and X-PHOS (0.46 mmol) in dioxane (5 mL) that had been stirred for 20 min was added to a stirred, degassed mixture of bis(pinacolato)diboron (9.2 mmol), potassium acetate (13.8 mmol) and compound **9** (4.6 mmol) in dioxane (50 mL). The mixture was stirred at 90 °C for 12 h. Upon completion, the reaction mixture was filtered and concentrated in vacuo. The residue was purified by silica gel column chromatography (dichloromethane/methanol, 200/1–60/1) to afford intermediate **10**.

4.2.3. Preparation of compound *12*

Substituted benzyl bromide (1.2 mmol) was added to a mixture of compound **11** (1 mmol) and K_2CO_3 (1.5 mmol) in DMF (5 mL), and the reaction mixture was stirred for 5 h at room temperature. The reaction solution was poured into water (60 mL). The suspension was filtered to yield compound **12**.

4.2.4. Preparation of compound *13*

$Pd(PPh_3)_4$ (0.05 mmol) was added to a mixture of compound **12** (1.2 mmol), compound **10** (1 mmol) and K_3PO_4 (2 mmol) in 4/1 dioxane/water mixture (15 mL). The mixture was degassed and placed under a nitrogen atmosphere and then stirred at 120 °C for 24 h. After cooling to room temperature, the mixture was extracted using ethyl acetate and water. The organic layer was separated, and the aqueous layer was extracted. The combined organic phases were washed with brine, dried and concentrated. The crude product was purified by silica gel column chromatography (dichloromethane/methanol, 150/1–50/1) to afford target compound **13**.

4-(4-amino-1-(2-fluorobenzyl)-1*H*-pyrazolo[3,4-*d*]pyrimidin-3-yl)-*N*-(pyridin-2-yl)benzamide (13a)

White solid, yield 67%, Mp: 204–207 °C, ^1H NMR (400 MHz, DMSO-d_6) δ 10.90 (s, 1H, NH), 8.41 (d, J = 3.9 Hz, 1H, Ar-H), 8.33 (s, 1H, Ar-H), 8.21 (t, J = 9.0 Hz, 3H, Ar-H), 7.86 (t, J = 7.7 Hz, 1H, Ar-H), 7.79 (d, J = 8.1 Hz, 2H, Ar-H), 7.44–6.97 (m, 7H, Ar-H and NH_2), 5.65 (s, 2H, CH_2). ^{13}C NMR (100 MHz, DMSO-d_6) δ 166.02, 160.34 (d, J =

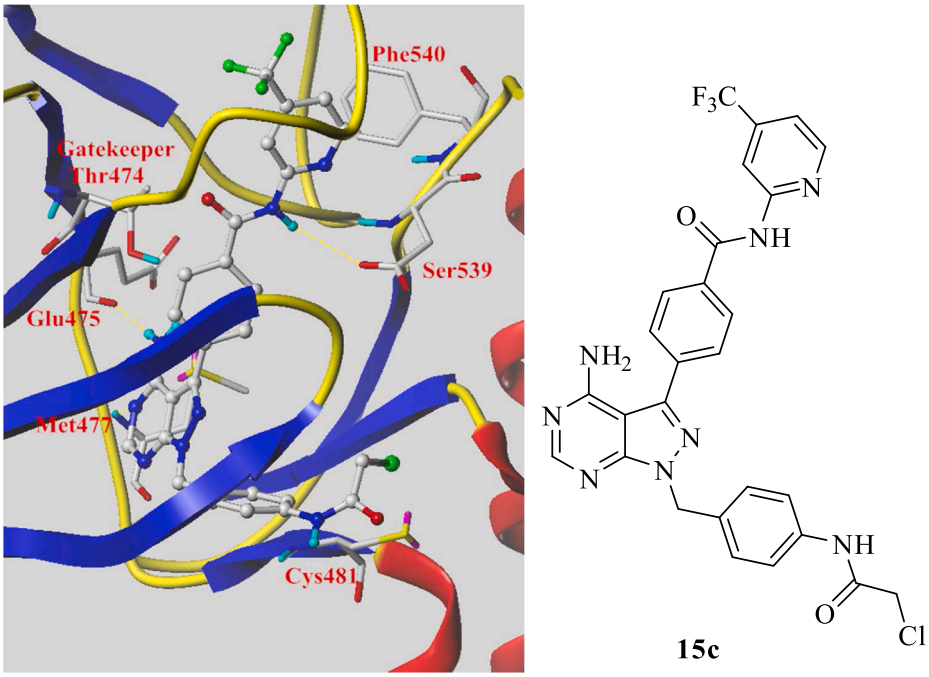

Fig. 4. Molecular docking mode of **15c** with BTK. (PDB ID: 5fbo).

245 Hz, 1C), 158.69, 156.61, 155.13, 152.61, 148.46, 143.96, 138.64, 136.38, 134.33, 130.66 (d, J = 3 Hz, 1C), 130.35 (d, J = 8 Hz, 1C), 129.31, 128.61, 125.14 (d, J = 3 Hz, 1C), 124.22 (d, J = 15 Hz, 1C), 120.38, 115.94 (d, J = 21 Hz, 1C), 115.26, 97.88, 44.10 (d, J = 4 Hz, 1C). MS(ESI) m/z: 440.27 $[M + H]^+$

4-(4-amino-1-(2-chlorobenzyl)-1*H*-pyrazolo [3,4-*d*] pyrimidin-3-yl)-*N*-(pyridin-2-yl) benzamide (13b)

White solid, yield 70%, Mp: 224–226 ℃, ^{1}H NMR (400 MHz, DMSO-d_6) δ 10.90 (s, 1H, NH), 8.42 (s, 1H, Ar-H), 8.31 (s, 1H, Ar-H), 8.24–8.20 (m, 3H, Ar-H), 7.92–7.76 (m, 3H, Ar-H), 7.64–6.75 (m, 7H, Ar-H and NH_2), 5.69 (s, 2H, CH_2). ^{13}C NMR (100 MHz, DMSO-d_6) δ 166.01, 158.74, 156.65, 155.37, 152.62, 148.46, 144.14, 138.64, 136.37, 134.78, 134.35, 132.38, 129.96, 129.91, 129.85, 129.32, 128.62, 128.01, 120.38, 115.26, 97.90, 47.92. MS(ESI) m/z: 456.14 $[M+H]^+$.

4-(4-amino-1-(2-bromobenzyl)-1*H*-pyrazolo [3,4-*d*] pyrimidin-3-yl)-*N*-(pyridin-2-yl) benzamide (13c)

White solid, yield 61%, Mp: 240–242 ℃, ^{1}H NMR (400 MHz, DMSO-d_6) δ 10.90 (s, 1H, NH), 8.41 (d, J = 4.5 Hz, 1H, Ar-H), 8.31 (s, 1H, Ar-H), 8.24–8.20 (m, 3H, Ar-H), 7.89–7.84 (m, 1H, Ar-H), 7.81 (d, J = 8.2 Hz, 2H, Ar-H), 7.68 (d, J = 7.8 Hz, 1H, Ar-H), 7.42–7.13 (m, 4H, Ar-H and NH_2), 7.12–6.69 (m, 2H, Ar-H and NH_2), 5.66 (s, 2H, CH_2). ^{13}C NMR (100 MHz, DMSO-d_6) δ 166.02, 158.74, 156.66, 155.41, 152.61, 148.46, 144.18, 138.64, 136.37, 134.37, 133.17, 130.16, 129.68, 129.31, 128.63, 128.55, 122.45, 120.39, 115.26, 97.92, 50.34. MS(ESI) m/z: 500.22 $[M+H]^+$.

4-(4-amino-1-(2-nitrobenzyl)-1*H*-pyrazolo [3,4-*d*] pyrimidin-3-yl)-*N*-(pyridin-2-yl)benzamide (13d)

White solid, yield 59%, Mp: 236–238 ℃, ^{1}H NMR (400 MHz, DMSO-d_6) δ 10.85 (s, 1H, NH), 8.41 (d, J = 3.9 Hz, 1H, Ar-H), 8.29 (s, 1H, Ar-H), 8.26–8.18 (m, 3H, Ar-H), 8.13 (d, J = 8.0 Hz, 1H, Ar-H), 7.86 (t, J = 8.7 Hz, 1H, Ar-H), 7.79 (d, J = 8.2 Hz, 2H, Ar-H), 7.68 (t, J = 7.4 Hz, 1H, Ar-H), 7.59 (t, J = 7.6 Hz, 1H, Ar-H), 7.47–6.59 (m, 4H, Ar-H and NH_2), 5.97 (s, 2H, CH_2). ^{13}C NMR (100 MHz, DMSO-d_6) δ 166.01, 158.77, 156.74, 155.54, 152.62, 148.45, 148.18, 144.40, 138.63, 136.27, 134.65, 134.43, 132.24, 129.86, 129.57, 129.32, 128.62, 125.46, 120.38, 115.26, 97.98, 47.42. MS(ESI) m/z: 467.05 $[M+H]^+$.

4-(4-amino-1-(3-nitrobenzyl)-1H-pyrazolo [3,4-d] pyrimidin-3-yl)-N-(pyridin-2-yl)benzamide (13e)

White solid, yield 69%, Mp: 225–228 ℃, ^{1}H NMR (400 MHz, DMSO-d_6) δ 10.86 (s, 1H, NH), 8.41 (d, J = 3.9 Hz, 1H, Ar-H), 8.34 (s, 1H, Ar-H), 8.23–8.20 (m, 4H, Ar-H), 8.16 (d, J = 8.1 Hz, 1H, Ar-H), 7.86 (t, J = 8.7 Hz, 1H, Ar-H), 7.81 (d, J = 8.3 Hz, 2H, Ar-H), 7.75 (d, J = 7.7 Hz, 1H, Ar-H), 7.65 (t, J = 7.9 Hz, 1H, Ar-H), 7.54 – 6.49 (m, 3H, Ar-H and NH_2), 5.77 (s, 2H, CH_2). ^{13}C NMR (100 MHz, DMSO-d_6) δ 166.01, 158.75, 156.77, 155.19, 152.61, 148.46, 148.32, 144.25, 139.68, 138.64, 136.29, 134.78, 134.40, 130.80, 129.33, 128.62, 123.17, 122.80, 120.39, 115.26, 97.98, 49.52. MS(ESI) m/z: 467.13 $[M+H]^+$.

4-(4-amino-1-(4-nitrobenzyl)-1*H*-pyrazolo [3,4-*d*] pyrimidin-3-yl)-*N*-(pyridin-2-yl)benzamide (13f)

White solid, yield 68%, Mp: 247–249 ℃, ^{1}H NMR (400 MHz, DMSO-d_6) δ 10.86 (s, 1H, NH), 8.41 (d, J = 4.6 Hz, 1H, Ar-H), 8.32 (s, 1H, Ar-H), 8.28 – 8.18 (m, 5H, Ar-H), 7.90 – 7.79 (m, 3H, Ar-H), 7.54 (d, J = 8.6 Hz, 2H, Ar-H), 7.42 – 6.49 (m, 3H, Ar-H and NH_2), 5.76 (s, 2H, CH_2). ^{13}C NMR (100 MHz, DMSO-d_6) δ 166.01, 158.74, 156.75, 155.24, 152.61, 148.46, 147.42, 145.08, 144.28, 138.64, 136.28, 134.39, 129.32, 129.17, 128.63, 124.32, 120.39, 115.26, 97.97, 49.72. MS(ESI) m/z: 467.11 $[M+H]^+$.

4-(4-amino-1-(2-fluorobenzyl)-1*H*-pyrazolo [3,4-*d*] pyrimidin-3-yl)-*N*-(4-methylpyridin-2-yl) benzamide (13g)

White solid, yield 71%, Mp: 212–215 ℃, ^{1}H NMR (400 MHz, DMSO-d_6) δ 10.80 (s, 1H, NH), 8.32 (s, 1H, Ar-H), 8.26 (d, J = 5.0 Hz, 1H, Ar-H), 8.19 (d, J = 8.2 Hz, 2H, Ar-H), 8.08 (s, 1H, Ar-H), 7.78 (d, J = 8.2 Hz, 2H, Ar-H), 7.37 (q, J = 6.1 Hz, 1H, Ar-H), 7.26–7.14 (m, 4H, Ar-H and NH_2), 7.11–6.63 (m, 2H, Ar-H and NH_2), 5.65 (s, 2H, CH_2), 2.37 (s, 3H, CH_3). ^{13}C NMR (100 MHz, DMSO-d_6) δ 165.92, 160.34 (d, J = 245 Hz, 1C), 158.69, 156.60, 155.13, 152.65, 149.33, 148.07, 143.97, 136.34, 134.39, 130.66 (d, J = 4 Hz, 1C), 130.44 (d, J = 8 Hz, 1C), 129.25, 128.60, 125.14 (d, J = 3 Hz, 1C), 124.23 (d, J = 15 Hz, 1C), 121.40, 115.94 (d, J = 21 Hz, 1C), 115.64, 97.87, 44.10 (d, J = 4 Hz, 1C), 21.42. MS(ESI) m/z: 454.10 $[M+H]^+$.

4-(4-amino-1-(2-chlorobenzyl)-1*H*-pyrazolo [3,4-*d*] pyrimidin-3-yl)-*N*-(4-methylpyridin-2-yl) benzamide (13h)

White solid, yield 73%, Mp: 226–228 ℃, ^{1}H NMR (400 MHz, DMSO-d_6) δ 10.80 (s, 1H, NH), 8.31 (s, 1H, Ar-H), 8.26 (d, J = 5.0 Hz, 1H, Ar-H), 8.19 (d, J = 8.3 Hz, 2H, Ar-H), 8.09 (s, 1H, Ar-H), 7.79 (d, J = 8.3 Hz, 2H, Ar-H), 7.52 (d, J = 7.8 Hz, 1H, Ar-H), 7.40–7.26 (m, 3H, Ar-H and NH_2), 7.04–7.01 (m, 3H, Ar-H and NH_2), 5.69 (s, 2H, CH_2), 2.37

(s, 3H, CH_3). ^{13}C NMR (100 MHz, DMSO-d_6) δ 165.92, 158.73, 156.65, 155.37, 152.65, 149.33, 148.08, 144.14, 136.32, 134.78, 134.42, 132.38, 129.96, 129.92, 129.86, 129.26, 128.62, 128.01, 121.40, 115.64, 97.89, 47.92, 21.43. MS(ESI) *m/z*: 470.14 $[M+H]^+$.

4-(4-amino-1-(2-bromobenzyl)-1*H*-pyrazolo [3,4-*d*] pyrimidin-3-yl)-*N*-(4-methylpyridin-2-yl) benzamide (13i)

White solid, yield 66%, Mp: 224 – 226 ℃, ^{1}H NMR (400 MHz, DMSO-d_6) δ 10.80 (s, 1H), 8.30 (s, 1H, Ar-H), 8.26 (d, J = 5.0 Hz, 1H, Ar-H), 8.19 (d, J = 8.3 Hz, 2H, Ar-H), 8.08 (s, 1H, Ar-H), 7.80 (d, J = 8.3 Hz, 2H, Ar-H), 7.68 (d, J = 7.8 Hz, 1H, Ar-H), 7.41 – 7.22 (m, 3H, Ar-H and NH_2), 7.09 – 6.88 (m, 3H, Ar-H and NH_2), 5.66 (s, 2H, CH_2), 2.37 (s, 3H, CH_3). ^{13}C NMR (100 MHz, DMSO-d_6) δ 170.82, 165.91, 158.72, 156.64, 155.39, 149.33, 148.07, 144.17, 136.36, 136.30, 134.41, 133.16, 130.17, 129.68, 129.25, 128.62, 128.56, 122.44, 121.40, 115.63, 97.90, 50.33, 21.43. MS(ESI) *m/z*: 513.97 $[M+H]^+$.

4-(4-amino-1-(2-nitrobenzyl)-1H-pyrazolo [3,4-d] pyrimidin-3-yl)-N-(4-methylpyridin-2-yl) benzamide (13j)

White solid, yield 72%, Mp: 228–231 ℃, ^{1}H NMR (400 MHz, DMSO-d_6) δ 10.80 (s, 1H, NH), 8.29 (s, 1H, Ar-H), 8.26 (d, J = 5.0 Hz, 1H, Ar-H), 8.20 (d, J = 8.3 Hz, 2H, Ar-H), 8.14 (d, J = 7.7 Hz, 1H, Ar-H), 8.09 (s, 1H, Ar-H), 7.79 (d, J = 8.2 Hz, 2H, Ar-H), 7.68 (t, J = 7.3 Hz, 1H, Ar-H), 7.59 (t, J = 7.5 Hz, 1H, Ar-H), 7.41–6.52 (m, 4H, Ar-H and NH_2), 5.97 (s, 2H, CH_2), 2.37 (s, 3H, CH_3). ^{13}C NMR (100 MHz, DMSO-d_6) δ 165.91, 158.76, 156.74, 155.53, 152.66, 149.32, 148.18, 148.07, 144.40, 136.22, 134.66, 134.48, 132.23, 129.85, 129.57, 129.26, 128.61, 125.46, 121.39, 115.63, 97.95, 47.40, 21.42. MS(ESI) *m/z*: 481.15 $[M+H]^+$.

4-(4-amino-1-(3-nitrobenzyl)-1H-pyrazolo [3,4-d] pyrimidin-3-yl)-N-(4-methylpyridin-2-yl) benzamide (13k)

White solid, yield 72%, Mp: 210–213 ℃, ^{1}H NMR (400 MHz, DMSO-d_6) δ 10.76 (s, 1H, NH), 8.34 (s, 1H, Ar-H), 8.26 (d, J = 5.0 Hz, 1H, Ar-H), 8.21–8.15 (m, 4H, Ar-H), 8.08 (s, 1H, Ar-H), 7.80 (d, J = 8.3 Hz, 2H, Ar-H), 7.75 (d, J = 7.7 Hz, 1H, Ar-H), 7.65 (t, J = 7.9 Hz, 1H, Ar-H), 7.50 – 6.36 (m, 3H, Ar-H and NH_2), 5.77 (s, 2H, CH_2), 2.37 (s, 3H, CH_3). ^{13}C NMR (100 MHz, DMSO-d_6) δ 165.91, 158.75, 156.76, 155.19, 152.65, 149.32, 148.32, 148.07, 144.25, 139.68, 136.24, 134.78, 134.46, 130.79, 129.27, 128.62, 123.16, 122.80, 121.39, 115.64, 97.98, 49.52, 21.42. MS(ESI) *m/z*: 481.11 $[M+H]^+$.

4-(4-amino-1-(4-nitrobenzyl)-1*H*-pyrazolo [3,4-*d*] pyrimidin-3-yl)-*N*-(4-methylpyridin-2-yl) benzamide (13l)

White solid, yield 71%, Mp: 222–225 ℃, ^{1}H NMR (400 MHz, DMSO-d_6) δ 10.80 (s, 1H, NH), 8.32 (s, 1H, Ar-H), 8.26 (d, J = 5.0 Hz, 1H, Ar-H), 8.22–8.19 (m, 4H, Ar-H), 8.08 (s, 1H, Ar-H), 7.80 (d, J = 8.2 Hz, 2H, Ar-H), 7.70–6.29 (m, 5H, Ar-H and NH_2), 5.76 (s, 2H, CH_2), 2.37 (s, 3H, CH_3). ^{13}C NMR (100 MHz, DMSO-d_6) δ 165.91, 158.74, 156.75, 155.24, 152.64, 149.33, 148.07, 147.42, 145.07, 144.29, 136.24, 134.45, 129.26, 129.16, 128.63, 124.31, 121.40, 115.64, 97.97, 49.71, 21.42. MS(ESI) *m/z*: 481.18 $[M+H]^+$.

4-(4-amino-1-(2-fluorobenzyl)-1H-pyrazolo [3,4-d] pyrimidin-3-yl)-N-(4-(trifluoromethyl) pyridin-2-yl)benzamide (13m)

White solid, yield 73%, Mp: 248–250 ℃, ^{1}H NMR (400 MHz, DMSO-d_6) δ 11.41 (s, 1H, NH), 8.70 (d, J = 5.1 Hz, 1H, Ar-H), 8.58 (s, 1H, Ar-H), 8.32 (s, 1H, Ar-H), 8.22 (d, J = 8.3 Hz, 2H, Ar-H), 7.81 (d, J = 8.3 Hz, 2H, Ar-H), 7.57 (d, J = 5.0 Hz, 1H, Ar-H), 7.40–7.34 (m, 1H, Ar-H), 7.32–6.73 (m, 5H, Ar-H and NH_2), 5.65 (s, 2H, CH_2). ^{13}C NMR (100 MHz, DMSO-d_6) δ 166.67, 160.34 (d, J = 244 Hz, 1C), 158.70, 156.61, 155.16, 153.72, 150.39, 143.89, 138.81 (q, J = 33 Hz, 1C), 136.74, 133.80, 130.65 (d, J = 4 Hz, 1C), 130.41 (d, J = 10 Hz, 1C), 129.46, 128.65, 125.12 (d, J = 4 Hz, 1C), 124.27 (d, J = 4 Hz, 1C), 123.43 (q, J = 272 Hz, 1C), 115.93 (d, J = 21 Hz, 1C), 115.66 (q, J = 3 Hz, 1C), 110.30 (q, J = 4 Hz, 1C), 97.91, 44.11 (d, J = 4 Hz, 1C). MS(ESI) *m/z*: 508.09 $[M+H]^+$.

4-(4-amino-1-(2-chlorobenzyl)-1H-pyrazolo [3,4-d] pyrimidin-3-yl)-N-(4-(trifluoromethyl) pyridin-2-yl)benzamide (13n)

Yellow solid, yield 71%, Mp: 210–212 ℃, ^{1}H NMR (400 MHz, DMSO-d_6) δ 11.40 (s, 1H, NH), 8.70 (d, J = 5.1 Hz, 1H, Ar-H), 8.58 (s, 1H, Ar-H), 8.31 (s, 1H, Ar-H), 8.22 (d, J = 8.2 Hz, 2H, Ar-H), 7.82 (d, J = 8.2 Hz, 2H, Ar-H), 7.56 (d, J = 4.4 Hz, 1H, Ar-H), 7.51 (d, J = 7.8 Hz, 1H, Ar-H), 7.44–7.15 (m, 3H, Ar-H and NH_2), 7.12–6.66 (m, 2H, Ar-H and NH_2), 5.69 (s, 2H, CH_2). ^{13}C NMR (100 MHz, DMSO-d_6) δ 166.68, 158.70, 156.60, 155.37, 153.72, 150.42, 144.08, 138.82 (q, J = 31 Hz, 1C), 136.71, 134.76, 133.83, 132.39, 129.97, 129.92, 129.88, 129.47, 128.68, 128.01, 123.43 (q, J = 272 Hz, 1C), 115.70 (q, J = 3 Hz, 1C), 110.30 (q, J = 4 Hz, 1C), 97.92, 47.94. MS(ESI) *m/z*: 524.08 $[M+H]^+$.

4-(4-amino-1-(2-bromobenzyl)-1H-pyrazolo [3,4-d] pyrimidin-3-yl)-N-(4-(trifluoromethyl) pyridin-2-yl)benzamide (13o)

Yellow solid, yield 65%, Mp: 218–220 ℃, ^{1}H NMR (400 MHz, DMSO-d_6) δ 11.41 (s, 1H, NH), 8.71 (d, J = 5.1 Hz, 1H, Ar-H), 8.58 (s, 1H, Ar-H), 8.31 (s, 1H, Ar-H), 8.22 (d, J = 8.2 Hz, 2H, Ar-H), 7.83 (d, J = 8.2 Hz, 2H, Ar-H), 7.69 (d, J = 7.8 Hz, 1H, Ar-H), 7.57 (d, J = 5.1 Hz, 1H, Ar-H), 7.39–6.63 (m, 5H, Ar-H and NH_2), 5.67 (s, 2H, CH_2). ^{13}C NMR (100 MHz, DMSO-d_6) δ 166.68, 158.74, 156.66, 155.42, 153.71, 150.41, 144.11, 138.81 (q, J = 33 Hz, 1C), 136.71, 136.35, 133.83, 133.17, 130.17, 129.69, 129.47, 128.68, 128.55, 123.42 (q, J = 272 Hz, 1C), 122.46, 115.68 (q, J = 4 Hz, 1C), 110.30 (q, J = 4 Hz, 1C), 97.93, 50.35. MS(ESI) *m/z*: 568.02 $[M+H]^+$.

-(4-amino-1-(2-nitrobenzyl)-1H-pyrazolo [3,4-d] pyrimidin-3-yl)-N-(4-(trifluoromethyl) pyridin-2-yl)benzamide (13p)

White solid, yield 55%, Mp: 105–108 ℃, ^{1}H NMR (400 MHz, DMSO-d_6) δ 11.39 (s, 1H, NH), 8.70 (d, J = 5.0 Hz, 1H, Ar-H), 8.58 (s, 1H, Ar-H), 8.30 (s, 1H, Ar-H), 8.23 (d, J = 7.8 Hz, 2H, Ar-H), 8.14 (d, J = 8.1 Hz, 1H, Ar-H), 7.82 (d, J = 7.8 Hz, 2H, Ar-H), 7.68 (t, J = 7.5 Hz, 1H, Ar-H), 7.61–6.52 (m, 5H, Ar-H and NH_2), 5.98 (s, 2H, CH_2). ^{13}C NMR (100 MHz, DMSO-d_6) δ 166.66, 158.76, 156.74, 155.55, 153.72, 150.39, 148.18, 144.32, 138.82 (q, J = 33 Hz, 1C), 136.62, 134.64, 133.89, 132.21, 129.85, 129.57, 129.47, 128.66, 125.45, 123.42 (q, J = 272 Hz, 1C), 115.66 (q, J = 3 Hz, 1C), 110.29 (q, J = 4 Hz, 1C), 97.98, 47.42. MS (ESI) *m/z*: 533.23 $[M-H]^-$.

4-(4-amino-1-(3-nitrobenzyl)-1H-pyrazolo [3,4-d] pyrimidin-3-yl)-N-(4-(trifluoromethyl) pyridin-2-yl)benzamide (13q)

White solid, yield 69%, Mp: 248–251 ℃, ^{1}H NMR (400 MHz, DMSO-d_6) δ 11.38 (s, 1H, NH), 8.69 (d, J = 4.7 Hz, 1H, Ar-H), 8.57 (s, 1H, Ar-H), 8.34 (s, 1H, Ar-H), 8.24 (s, 1H, Ar-H), 8.22 (s, 2H, Ar-H), 8.15 (d, J = 7.9 Hz, 1H, Ar-H), 7.83 (d, J = 7.8 Hz, 2H, Ar-H), 7.74 (d, J = 7.4 Hz, 1H, Ar-H), 7.64 (t, J = 7.8 Hz, 1H, Ar-H), 7.54 (d, J = 4.4 Hz, 1H, Ar-H), 7.44–6.20 (s, 2H, NH_2), 5.77 (s, 2H, CH_2). ^{13}C NMR (100 MHz, DMSO-d_6) δ 166.64, 158.75, 156.75, 155.21, 153.71, 150.35, 148.30, 144.18, 139.64, 138.81 (q, J = 33 Hz, 1C), 136.64, 134.75, 133.87, 130.74, 129.48, 128.66, 123.41 (q, J = 271 Hz, 1C), 123.12, 122.80, 115.62 (q, J = 3 Hz, 1C), 110.29 (q, J = 4 Hz, 1C), 98.01, 49.54. MS(ESI) *m/z*: 533.40 $[M-H]^-$.

4-(4-amino-1-(4-nitrobenzyl)-1H-pyrazolo [3,4-d] pyrimidin-3-yl)-N-(4-(trifluoromethyl) pyridin-2-yl)benzamide (13r)

White solid, yield 68%, Mp: 224–227 ℃, ^{1}H NMR (400 MHz, DMSO-d_6) δ 11.40 (s, 1H, NH), 8.64 (d, J = 47.2 Hz, 2H, Ar-H), 8.33–8.22 (m, 6H, Ar-H), 7.84 (s, 2H, Ar-H), 7.55 (s, 3H, Ar-H and NH_2), 7.05 (br, s, 1H, NH_2), 5.77 (s, 2H, CH_2). ^{13}C NMR (100 MHz, DMSO-d_6) δ 166.65, 158.75, 156.75, 155.27, 153.72, 150.37, 147.43, 145.04, 144.22, 138.82 (q, J = 33 Hz, 1C), 136.65, 133.86, 129.47, 129.16, 128.68, 124.29, 123.42 (q, J = 272 Hz, 1C), 115.64 (q, J = 3 Hz, 1C), 110.30 (q, J = 5 Hz, 1C), 98.01, 49.73. MS(ESI) *m/z*: 533.57 $[M-H]^-$.

*4.2.5. Preparation of compounds **14***

Compound 13 with a nitro group (1.00 mmol) was added to a mixture of Fe (3 mmol) and NH_4Cl (3 mmol) in 3/1 ethanol/water mixture (20 mL). Then, the mixture was stirred at 90 °C for 6 h. The reaction mixture was hot filtered, and the filtrate was concentrated under reduced pressure. The crude product was purified by silica gel column chromatography (dichloromethane/methanol, 120/1–30/1) to afford target compound **14**.

4-(4-amino-1-(2-aminobenzyl)-1H-pyrazolo [3,4-d] pyrimidin-

3-yl)-N-(pyridin-2-yl)benzamide (14a)

White solid, yield 63%, Mp: 250–253 ℃, ^{1}H NMR (400 MHz, DMSO-d_6) δ 10.90 (s, 1H, NH), 8.41 (d, J = 4.1 Hz, 1H, Ar-H), 8.33 (s, 1H, Ar-H), 8.24–8.20 (m, 3H, Ar-H), 7.86 (t, J = 7.3 Hz, 1H, Ar-H), 7.80 (d, J = 8.1 Hz, 2H, Ar-H), 7.34–6.44 (m, 7H, Ar-H and NH_2), 5.42 (s, 2H, CH_2), 5.39 (s, 2H, NH_2). ^{13}C NMR (100 MHz, DMSO-d_6) δ 166.02, 158.74, 156.49, 154.69, 152.62, 148.46, 146.90, 143.54, 138.63, 136.40, 134.31, 130.21, 129.32, 129.22, 128.57, 120.52, 120.38, 116.70, 115.74, 115.27, 97.78, 47.63. HRMS(ESI) *m/z* calcd for $C_{24}H_{20}N_8O$ $[M + H]^+$ 437.1833, found 437.1833.

4-(4-amino-1-(3-aminobenzyl)-1*H*-pyrazolo [3,4-*d*] pyrimidin-3-yl)-*N*-(pyridin-2-yl)benzamide (14b)

White solid, yield 61%, Mp: 226–229 ℃, ^{1}H NMR (400 MHz, DMSO-d_6) δ 10.89 (s, 1H, NH), 8.41 (d, J = 3.9 Hz, 1H, Ar-H), 8.31 (s, 1H, Ar-H), 8.24–8.20 (m, 3H, Ar-H), 7.87 (t, J = 7.8 Hz, 1H, Ar-H), 7.80 (d, J = 8.3 Hz, 2H, Ar-H), 7.54–6.65 (m, 4H, Ar-H and NH_2), 6.47–6.44 (m, 3H, Ar-H), 5.42 (s, 2H, CH_2), 5.10 (s, 2H, NH_2). ^{13}C NMR (100 MHz, DMSO-d_6) δ 166.03, 158.66, 156.48, 154.93, 152.63, 149.36, 148.46, 143.46, 138.63, 138.08, 136.57, 134.22, 129.49, 129.30, 128.59, 120.37, 115.46, 115.27, 113.61, 113.21, 97.88, 50.68. HRMS(ESI) *m/z* calcd for $C_{24}H_{20}N_8O$ $[M + H]^+$ 437.1833, found 437.1833.

4-(4-amino-1-(4-aminobenzyl)-1*H*-pyrazolo [3,4-*d*] pyrimidin-3-yl)-*N*-(pyridin-2-yl)benzamide (14c)

White solid, yield 72%, Mp: 224–227 ℃, ^{1}H NMR (400 MHz, DMSO-d_6) δ 10.89 (s, 1H, NH), 8.41 (d, J = 4.7 Hz, 1H, Ar-H), 8.31 (s, 1H, Ar-H), 8.24–8.19 (m, 3H, Ar-H), 7.86 (t, J = 8.6 Hz, 1H, Ar-H), 7.78 (d, J = 8.2 Hz, 2H, Ar-H), 7.52–6.60 (m, 5H, Ar-H and NH_2), 6.49 (d, J = 8.3 Hz, 2H, Ar-H), 5.38 (s, 2H, CH_2), 5.07 (s, 2H, NH_2). ^{13}C NMR (100 MHz, DMSO-d_6) δ 166.03, 158.62, 156.38, 154.61, 152.63, 148.79, 148.46, 143.23, 138.63, 136.63, 134.17, 129.43, 129.29, 128.56, 124.30, 120.37, 115.27, 114.14, 97.92, 50.38. HRMS(ESI) *m/z* calcd for $C_{24}H_{20}N_8O$ $[M + H]^+$ 437.1833, found 437.1831.

4-(4-amino-1-(2-aminobenzyl)-1*H*-pyrazolo [3,4-*d*] pyrimidin-3-yl)-*N*-(4-methylpyridin-2-yl)benzamide (14d)

White solid, yield 68%, Mp: 205–208 ℃, ^{1}H NMR (400 MHz, DMSO-d_6) δ 10.76 (s, 1H, NH), 8.33 (s, 1H, Ar-H), 8.26 (d, J = 5.0 Hz, 1H, Ar-H), 8.19 (d, J = 8.3 Hz, 2H, Ar-H), 8.08 (s, 1H, Ar-H), 7.79 (d, J = 8.3 Hz, 2H, Ar-H), 7.36–6.45 (m, 7H, Ar-H and NH_2), 5.41 (s, 2H, CH_2), 5.37 (s, 2H, NH_2), 2.37 (s, 3H, CH_3). ^{13}C NMR (100 MHz, DMSO-d_6) δ 165.91, 158.75, 156.48, 154.69, 152.66, 149.30, 148.06, 146.91, 143.54, 136.36, 134.38, 130.23, 129.28, 129.22, 128.57, 121.38, 120.54, 116.70, 115.76, 115.65, 97.78, 45.84, 21.41. HRMS(ESI) *m/z* calcd for $C_{25}H_{22}N_8O$ $[M+H]^+$ 451.1989, found 451.1986.

4-(4-amino-1-(3-aminobenzyl)-1*H*-pyrazolo [3,4-*d*] pyrimidin-3-yl)-*N*-(4-methylpyridin-2-yl)benzamide (14e)

White solid, yield 68%, Mp: 224–226 ℃, ^{1}H NMR (400 MHz, DMSO-d_6) δ 10.81 (s, 1H, NH), 8.32 (s, 1H, Ar-H), 8.26 (d, J = 4.8 Hz, 1H, Ar-H), 8.20 (d, J = 7.9 Hz, 2H, Ar-H), 8.09 (s, 1H, Ar-H), 7.80 (d, J = 8.0 Hz, 2H, Ar-H), 7.46–6.24 (m, 7H, Ar-H and NH_2), 5.42 (s, 2H, CH_2), 5.11 (s, 2H, NH_2), 2.37 (s, 3H, CH_3). ^{13}C NMR (100 MHz, DMSO-d_6) δ 165.94, 158.66, 156.47, 154.92, 152.66, 149.36, 149.32, 148.07, 143.46, 138.08, 136.53, 134.28, 129.50, 129.24, 128.59, 121.40, 115.65, 115.47, 113.61, 113.22, 97.87, 50.67, 21.43. HRMS(ESI) *m/z* calcd for $C_{25}H_{22}N_8O$ $[M+H]^+$ 451.1989, found 451.1978.

4-(4-amino-1-(4-aminobenzyl)-1*H*-pyrazolo [3,4-*d*] pyrimidin-3-yl)-*N*-(4-methylpyridin-2-yl)benzamide (14f)

Yellow solid, yield 58%, Mp: 188–192 ℃, ^{1}H NMR (400 MHz, DMSO-d_6) δ 10.80 (s, 1H, NH), 8.31 (s, 1H, Ar-H), 8.26 (d, J = 5.0 Hz, 1H, Ar-H), 8.19 (d, J = 8.3 Hz, 2H, Ar-H), 8.08 (s, 1H, Ar-H), 7.77 (d, J = 8.3 Hz, 2H, Ar-H), 7.43–6.30 (m, 7H, Ar-H and NH_2), 5.37 (s, 2H, CH_2), 5.11 (s, 2H, NH_2), 2.37 (s, 3H, CH_3). ^{13}C NMR (100 MHz, DMSO-d_6) δ 165.93, 158.61, 156.38, 154.61, 152.66, 149.30, 148.80, 148.08, 143.23, 136.58, 134.23, 129.42, 129.24, 128.55, 124.28, 121.39, 115.65, 114.13, 97.90, 50.37, 21.43. HRMS(ESI) *m/z* calcd for $C_{25}H_{22}N_8O$ $[M + H]^+$ 451.1989, found 451.1998.

4-(4-amino-1-(2-aminobenzyl)-1*H*-pyrazolo [3,4-*d*] pyrimidin-3-yl)-*N*-(4-(trifluoromethyl) pyridin-2-yl)benzamide (14g)

White solid, yield 69%, Mp: 240–243 ℃, ^{1}H NMR (400 MHz, DMSO-d_6) δ 11.40 (s, 1H, NH), 8.70 (d, J = 5.1 Hz, 1H, Ar-H), 8.58 (s, 1H, Ar-H), 8.34 (s, 1H, Ar-H), 8.23 (d, J = 7.8 Hz, 2H, Ar-H), 7.82 (d, J = 7.9 Hz, 2H, Ar-H), 7.56 (d, J = 5.0 Hz, 1H, Ar-H), 7.45–6.32 (m, 6H, Ar-H and NH_2), 5.42 (s, 2H, CH_2), 5.40 (s, 2H, NH_2). ^{13}C NMR (100 MHz, DMSO-d_6) δ 166.69, 158.75, 156.49, 154.71, 153.73, 150.41, 146.90, 143.47, 138.81 (q, J = 33 Hz, 1C), 136.76, 133.78, 130.21, 129.48, 129.22, 128.62, 123.43 (q, J = 272 Hz, 1C), 120.52, 116.70, 116.70, 115.75, 115.67 (q, J = 3 Hz, 1C), 110.31 (q, J = 4 Hz, 1C), 97.80, 47.64. HRMS(ESI) *m/z* calcd for $C_{25}H_{19}F_3N_8O$ $[M + H]^+$ 505.1707, found 505.1725.

4-(4-amino-1-(3-aminobenzyl)-1*H*-pyrazolo [3,4-*d*] pyrimidin-3-yl)-*N*-(4-(trifluoromethyl) pyridin-2-yl)benzamide (14h)

White solid, yield 73%, Mp: 240–242 ℃, ^{1}H NMR (400 MHz, DMSO-d_6) δ 11.32 (s, 1H, NH), 8.63 (d, J = 4.8 Hz, 1H, Ar-H), 8.51 (s, 1H, Ar-H), 8.25 (s, 1H, Ar-H), 8.16 (d, J = 7.9 Hz, 2H, Ar-H), 7.76 (d, J = 7.9 Hz, 2H, Ar-H), 7.48 (d, J = 4.5 Hz, 1H, Ar-H), 7.31–6.65 (m, 3H, Ar-H and NH_2), 6.40 (s, 3H, Ar-H), 5.35 (s, 2H, CH_2), 5.03 (s, 2H, NH_2). ^{13}C NMR (100 MHz, DMSO-d_6) δ 166.70, 158.67, 156.48, 154.95, 153.73, 150.40, 149.36, 143.39, 138.81 (q, J = 33 Hz, 1C), 138.07, 136.93, 133.70, 129.49, 129.46, 128.65, 123.43 (q, J = 271 Hz, 1C), 115.65 (q, J = 3 Hz, 1C), 115.48, 113.63, 113.23, 110.31 (q, J = 4 Hz, 1C), 97.91, 50.69. HRMS(ESI) *m/z* calcd for $C_{25}H_{19}F_3N_8O$ $[M + H]^+$ 505.1707, found 505.1712.

4-(4-amino-1-(4-aminobenzyl)-1*H*-pyrazolo [3,4-*d*] pyrimidin-3-yl)-*N*-(4-(trifluoromethyl) pyridin-2-yl)benzamide (14i)

White solid, yield 75%, Mp: 266–269 ℃, ^{1}H NMR (400 MHz, DMSO-d_6) δ 11.38 (s, 1H, NH), 8.69 (d, J = 5.0 Hz, 1H, Ar-H), 8.58 (s, 1H, Ar-H), 8.32 (s, 1H, Ar-H), 8.22 (d, J = 7.5 Hz, 2H, Ar-H), 7.80 (d, J = 7.6 Hz, 2H, Ar-H), 7.55 (d, J = 5.0 Hz, 1H, Ar-H), 7.37–6.74 (m, 4H, Ar-H and NH_2), 6.50 (d, J = 7.5 Hz, 2H, Ar-H), 5.38 (s, 2H, CH_2), 5.07 (s, 2H, NH_2). ^{13}C NMR (100 MHz, DMSO-d_6) δ 166.74, 158.63, 156.39, 154.64, 153.94, 150.40, 148.79, 143.18, 138.76 (q, J = 33 Hz, 1C), 136.94, 133.79, 129.45, 129.43, 128.60, 123.45 (q, J = 272 Hz, 1C), 124.30, 115.54 (q, J = 3 Hz, 1C), 114.15, 110.35 (q, J = 4 Hz, 1C), 97.94, 50.40. HRMS(ESI) *m/z* calcd for $C_{25}H_{19}F_3N_8O$ $[M + H]^+$ 505.1707, found 505.1707.

*4.2.6. Preparation of compounds **15***

To a solution of **14** (0.5 mmol) and Et_3N (3 mmol) in THF (10 mL), acryloyl chloride or chloroacetyl chloride (1.2 mmol) was added under ice-cold conditions. The mixture was stirred at room temperature for 5 h. Upon completion, the mixture was extracted with ethyl acetate. The combined organic phases were washed with water and brine, then dried and concentrated. The crude product was purified by column chromatography (dichloromethane/methanol, 80/1–40/1) yielding target compounds **15**.

4-(4-amino-1-(3-(2-chloroacetamido)benzyl)-1*H*-pyrazolo [3,4-*d*] pyrimidin-3-yl)-*N*-(4-(trifluoromethyl)pyridin-2-yl)benzamide (15a)

White solid, yield 60%, Mp: 166–168 ℃, ^{1}H NMR (400 MHz, DMSO-d_6) δ 11.40 (s, 1H, NH), 10.32 (s, 1H, NH), 8.70 (d, J = 4.6 Hz, 1H, Ar-H), 8.58 (s, 1H, Ar-H), 8.34 (s, 1H, Ar-H), 8.23 (d, J = 7.7 Hz, 2H, Ar-H), 7.83 (d, J = 7.6 Hz, 2H, Ar-H), 7.57 (s, 2H, Ar-H), 7.48 (s, 1H, Ar-H), 7.40–6.67 (m, 4H, Ar-H and NH_2), 5.58 (s, 2H, CH_2), 4.22 (s, 2H, CH_2). ^{13}C NMR (100 MHz, DMSO-d_6) δ 166.69, 165.13, 158.50, 156.33, 154.96, 153.73, 150.42, 143.81, 139.23, 138.81 (q, J = 33 Hz, 1C), 138.21, 136.76, 133.80, 129.64, 129.48, 128.68, 123.66, 123.43 (q, J = 271 Hz, 1C), 119.07, 118.75, 115.69 (q, J = 4 Hz, 1C), 110.31 (q, J = 3 Hz, 1C), 97.92, 50.38, 44.01. HRMS(ESI) *m/z* calcd for $C_{27}H_{20}ClF_3N_8O_2$ $[M + H]^+$ 581.1423, found 581.1423.

4-(1-(3-acrylamidobenzyl)-4-amino-1*H*-pyrazolo [3,4-*d*] pyrimidin-3-yl)-*N*-(4-(trifluoromethyl) pyridin-2-yl)benzamide (15b)

White solid, yield 62%, Mp: 278–281 ℃, ^{1}H NMR (400 MHz, DMSO-d_6) δ 11.36 (s, 1H, NH), 10.17 (s, 1H, NH), 8.69 (d, J = 5.0 Hz,

1H, Ar-H), 8.57 (s, 1H, Ar-H), 8.50 (d, $J = 8.4$ Hz, 2H, Ar-H), 8.46 (s, 1H, Ar-H), 8.12 (d, $J = 8.4$ Hz, 2H, Ar-H), 7.81 – 7.44 (m, 4H, Ar-H and NH_2), 7.43 – 6.87 (m, 3H, Ar-H and NH_2), 6.41 (dd, $J = 17.0$, 10.1 Hz, 1H, CH), 6.24 (d, $J = 16.9$ Hz, 1H, CH_2), 5.74 (d, $J = 10.0$ Hz, 1H, CH_2), 5.61 (s, 2H, CH_2). ^{13}C NMR (100 MHz, DMSOd_6) δ 166.69, 163.66, 158.68, 156.58, 155.02, 153.72, 150.40, 143.70, 139.81, 138.80 (q, $J =$ 33 Hz, 1C), 138.10, 136.83, 133.76, 132.31, 129.50, 129.47, 128.68, 127.33, 123.42 (q, $J = 272$ Hz, 1C), 123.30, 119.08, 118.79, 115.66 (q, $J = 3$ Hz, 1C), 110.30 (q, $J = 4$ Hz, 1C), 97.94, 50.42. HRMS(ESI) *m/z* calcd for $C_{28}H_{21}F_3N_8O_2$ $[M + H]^+$ 559.1812, found 559.1816.

4-(4-amino-1-(4-(2-chloroacetamido)benzyl)-1*H*-pyrazolo [3,4-*d*] pyrimidin-3-yl)-*N*-(4-(trifluoromethyl)pyridin-2-yl)benzamide (15c)

Gray solid, yield 59%, Mp: 140–143 ℃, ^{1}H NMR (400 MHz, DMSO-d_6) δ 11.40 (s, 1H, NH), 10.34 (s, 1H, NH), 8.70 (d, $J = 4.9$ Hz, 1H, Ar-H), 8.58 (s, 1H, Ar-H), 8.33 (s, 1H, Ar-H), 8.23 (d, $J = 8.0$ Hz, 2H, Ar-H), 7.83 (d, $J = 8.0$ Hz, 2H, Ar-H), 7.56 (d, $J = 7.2$ Hz, 3H, Ar-H), 7.32 (d, $J = 8.2$ Hz, 2H, Ar-H), 7.26–6.20 (s, 2H, NH_2), 5.56 (s, 2H, CH_2), 4.24 (s, 2H, CH_2). ^{13}C NMR (100 MHz, DMSO-d_6) δ 166.68, 165.09, 158.62, 156.47, 154.91, 153.73, 150.40, 143.65, 138.81 (q, $J =$ 33 Hz, 1C), 138.40, 136.83, 133.75, 132.86, 129.46, 128.84, 128.66, 123.43 (q, $J = 272$ Hz, 1C), 120.01, 115.64 (q, $J = 3$ Hz, 1C), 110.31 (q, $J = 4$ Hz, 1C), 97.96, 50.06, 43.99. HRMS(ESI) *m/z* calcd for $C_{27}H_{20}ClF_3N_8O_2$ $[M + H]^+$ 581.1423, found 581.1425.

4-(1-(4-acrylamidobenzyl)-4-amino-1*H*-pyrazolo [3,4-*d*] pyrimidin-3-yl)-*N*-(4-(trifluoromethyl) pyridin-2-yl)benzamide (15d)

White solid, yield 65%, Mp: 125–128 ℃, ^{1}H NMR (400 MHz, DMSO-d_6) δ 11.40 (s, 1H, NH), 10.19 (s, 1H, NH), 8.70 (d, $J = 4.6$ Hz, 1H, Ar-H), 8.59 (s, 1H, Ar-H), 8.34 (s, 1H, Ar-H), 8.23 (d, $J = 7.8$ Hz, 2H, Ar-H), 7.83 (d, $J = 7.7$ Hz, 2H, Ar-H), 7.65–7.55 (m, 4H, Ar-H), 7.42–6.82 (m, 3H, Ar-H and NH_2), 6.47–6.40 (m, 1H, CH), 6.25 (d, $J = 16.9$ Hz, 1H, CH_2), 5.75 (d, $J = 10.0$ Hz, 1H, CH_2), 5.56 (s, 2H, CH_2). ^{13}C NMR (100 MHz, DMSO-d_6) δ 166.68, 163.58, 158.69, 156.55, 154.92, 153.73, 150.39, 143.60, 138.97, 138.78 (q, $J = 29$ Hz, 1C), 136.86, 133.73, 132.49, 132.27, 129.46, 128.79, 128.66, 127.37, 123.43 (q, $J = 272$ Hz, 1C), 119.95, 115.65 (q, $J = 3$ Hz, 1C), 110.31 (q, $J = 4$ Hz, 1C), 97.97, 50.10. HRMS(ESI) *m/z* calcd for $C_{28}H_{21}F_3N_8O_2$ $[M + H]^+$ 559.1812, found 559.1806.

4.3. In vitro kinase activity assay

The *in vitro* BTK kinase activity and kinases selectivity activities were evaluated via a radiometric protein kinase assay following the protocol as previously described [30].

4.4. Cell antiproliferation assay

MCL cell lines Mino, Rec-1, Maver-1 and Z138 were purchased from the American Type Culture Collection (ATCC). Cell antiproliferation assays were performed on the MCL cell lines using a CellTiter-Glo luminescent cell viability assay kit (Promega) following a protocol previously described [31]. Briefly, cells were plated in 96-well plates at a density of 1×10^4 cells per well and then treated with different concentrations of target compounds and DMSO (control) and incubated in a humidified atmosphere with 5% CO_2 at 37 °C for 72 h. Cells were lysed with 30 μL of Cell Titer-Glo luminescent cell viability assay reagent, and the luminescence was quantified using a BioTek Synergy HTX multi-mode microplate reader. Each triplicate experiment was performed no less than three times to establish the cell survival curve. IC_{50} values were calculated with GraphPad Prism 6 software.

4.5. Western blotting

Z138 cells were cultured with different concentrations of **15c** and ibrutinib for 24 h. Then, cells were harvested and lysed in lysis buffer (Cell Signaling, Danvers, MA). The cell lysates were maintained on ice for 30 min and centrifuged at 12,000 × rpm for 20 min at 4 °C. The protein concentration was determined by Bradford assay (Bio-Rad, Hercules, CA). Twenty micrograms of sample protein was mixed with 4 × loading buffer and separated by 10% SDS-PAGE. The proteins were then transferred onto methanol-equilibrated PVDF membranes (Bio-Rad Laboratories, 162e0177), which were blocked for 1 h in 5% nonfat dry milk in TBST (BD Bioscience, San Jose, CA). The membranes were incubated with a primary antibody overnight at 4 °C. Secondary antibodies were added for 1 h at room temperature. Finally, the membrane was visualized by ECL (Perkin Elmer Life Sciences, NE104001EA). Antibodies against BTK, PLCγ2, p-BTK, p-PLCγ2, LC3B-II, β-actin and GAPDH were obtained from Cell Signaling.

4.6. Cell apoptosis assay

Apoptosis was quantified by Annexin V/PI-binding assay. Cells were seeded in 6-well plates containing **15c** at concentrations of 250 nM, 500 nM, or 1000 nM and incubated for 24 h. Treated cells were washed twice with cold phosphate-buffered saline (PBS) and then resuspended in 100 μL of binding buffer, to which 2 μL of Annexin V-FITC and 5 μL of PI were added. The samples were gently vortexed and incubated for 15 min at room temperature in the dark. After 200 μL of binding buffer was added, the samples were immediately analyzed by flow cytometry using a FACScan flow cytometer (Becton Dickinson, San Jose, CA). The number of apoptotic cells was determined using FlowJo software.

4.7. ROS assay

Intracellular ROS levels were measured by detecting the conversion of DCFH-DA to fluorescent DCF. Z138 cells were seeded in 6-well plates and treated with 1 μM test compound (ibrutinib or **15c**) for different times (12 h or 24 h). Then, the cells were collected and washed with PBS three times. After washing, the cells were incubated with DCFH-DA at 37 °C for 20 min. Then, the DCF fluorescence distribution was observed under a confocal laser scanning microscope (Leica TCS SP8) using an excitation wavelength of 488 nm and an emission wavelength of 525 nm.

4.8. Molecular docking analysis

Molecular docking analysis was performed using Sybyl 2.0 software, and the BTK crystal structure (PDB: 5fbo) was retrieved from the Protein Data Bank. Protein preparation was performed by extracting the ligand, removing water molecules, adding hydrogen atoms and assigning AMBER7 FF99 charges to the protein. Compound **15c** was docked into BTK, hydrogen bonds and hydrophobic interactions were observed in the model, and the best conformation with the highest CScore was selected for interaction analysis.

Declaration of Competing Interest

The authors declare that there is no conflict of interest.

Acknowledgements

This work was supported by the National Natural Science Foundation of China (No. 82073708).

Appendix A. Supplementary material

Supplementary data to this article can be found online at https://doi.org/10.1016/j.bioorg.2021.104968.

References

[1] J.M. Vose, Mantle cell lymphoma: 2017 update on diagnosis, risk-stratification, and clinical management, Am. J. Hematol. 92 (2017) 806-813. https://doi.org/10.1002/ajh.24797.

[2] P. Perez-Galan, M. Dreyling, A. Wiestner, Mantle cell lymphoma: biology, pathogenesis, and the molecular basis of treatment in the genomic era, Blood 117 (2011) 26-38. https://doi.org/ 10.1182/blood-2010-04-189977.

[3] M.I. Merolle, M. Ahmed, K. Nomie, M.L. Wang, The B cell receptor signaling pathway in mantle cell lymphoma, Oncotarget 9 (2018) 25332-25341, https://doi.org/ 10.18632/oncotarget.25011.

[4] A. Aalipour, R.H. Advani, Bruton tyrosine kinase inhibitors: a promising novel targeted treatment for B cell lymphomas, Br. J. Haematol. 163 (2013) 436-443, https://doi.org/ 10.1111/bjh.12573.

[5] J. Wu, C. Liu, S.T. Tsui, D. Liu, Second-generation inhibitors of Bruton tyrosine kinase, J. Hematol. Oncol. 9 (2016) 80, https://doi.org/ 10.1186/s13045-016-0313-y.

[6] O. Hershkovitz-Rokah, D. Pulver, G. Lenz, O. Shpilberg, Ibrutinib resistance in mantle cell lymphoma: clinical, molecular and treatment aspects, Br. J. Haematol. 181 (2018) 306–319, https://doi.org/10.1111/bjh.15108.

[7] A. Aw, J.R. Brown, Current status of Bruton's tyrosine kinase inhibitor development and use in B-cell malignancies, Drugs Aging 34 (2017) 509–527, https://doi.org/10.1007/s40266-017-0468-4.

[8] Z.Y. Pan, H. Scheerens, S.J. Li, B.E. Schultz, P.A. Sprengeler, L.C. Burrill, R. V. Mendonca, M.D. Sweeney, K.C.K. Scott, P.G. Grothaus, D.A. Jeffery, J. M. Spoerke, L.A. Honigberg, P.R. Young, S.A. Dalrymple, J.T. Palmer, Discovery of selective irreversible inhibitors for Bruton's tyrosine kinase, ChemMedChem 2 (2007) 58–61, https://doi.org/10.1002/cmdc.200600221.

[9] M.L. Wang, S. Rule, P. Martin, A. Goy, R. Auer, B.S. Kahl, W. Jurczak, R.H. Advani, J.E. Romaguera, M.E. Williams, J.C. Barrientos, E. Chmielowska, J. Radford, S. Stilgenbauer, M. Dreyling, W.W. Jedrzejczak, P. Johnson, S.E. Spurgeon, L. Li, L. Zhang, K. Newberry, Z.S. Ou, N. Cheng, B.L. Fang, J. McGreivy, F. Clow, J. J. Buggy, B.Y. Chang, D.M. Beaupre, L.A. Kunkel, K.A. Blum, Targeting BTK with ibrutinib in relapsed or refractory mantle-cell lymphoma, New Engl. J. Med. 369 (2013) 507–516, https://doi.org/10.1056/NEJMoa1306220.

[10] A. Noy, S. de Vos, C. Thieblemont, P. Martin, C.R. Flowers, F. Morschhauser, G. P. Collins, S. Ma, M. Coleman, S. Peles, S. Smith, J.C. Barrientos, A. Smith, B. Munneke, I. Dimery, D.M. Beaupre, R. Chen, Targeting BTK with ibrutinib in relapsed/ refractory marginal zone lymphoma, Blood 129 (2017) 2224–2232, https://doi.org/10.1182/blood-2016-10-747345.

[11] Y. Guo, Y. Liu, N. Hu, D. Yu, C. Zhou, G. Shi, B. Zhang, M. Wei, J. Liu, L. Luo, Z. Tang, H. Song, Y. Guo, X. Liu, D. Su, S. Zhang, X. Song, X. Zhou, Y. Hong, S. Chen, Z. Cheng, S. Young, Q. Wei, H. Wang, Q. Wang, L. Lv, F. Wang, H. Xu, H. Sun, H. Xing, N. Li, W. Zhang, Z. Wang, G. Liu, Z. Sun, D. Zhou, W. Li, L. Liu, L. Wang, Z. Wang, Discovery of zanubrutinib (BGB-3111), a novel, potent, and selective covalent inhibitor of Bruton's tyrosine kinase, J. Med. Chem. 62 (2019) 7923–7940, https://doi.org/10.1021/acs.jmedchem.9b00687.

[12] C. Owen, N.L. Berinstein, A. Christofides, L.H. Sehn, Review of Bruton tyrosine kinase inhibitors for the treatment of relapsed or refractory mantle cell lymphoma, Curr. Oncol. 26 (2019) e233–e240, https://doi.org/10.3747/co.26.4345.

[13] L. Jiahui, W. Jingde, H. Feng, Q. Ying, Z. Qiuqiong, Y. Chenggong, Development of Bruton's tyrosine kinase inhibitors for rheumatoid arthritis, Curr. Med. Chem. 25 (2018) 5847–5859, https://doi.org/10.2174/0929867325666180316121951.

[14] C. Liang, D. Tian, X. Ren, S. Ding, M. Jia, M. Xin, S. Thareja, The development of Bruton's tyrosine kinase (BTK) inhibitors from 2012 to 2017: A mini-review, Eur. J. Med. Chem. 151 (2018) 315-326, https://doi.org/10.1016/j.ejmech.2018.03.062.

[15] https://www.fda.gov/news-events/press-announcements/fda-approves-therapy-treat-patients-relapsed-and-refractory-mantle-cell-lymphoma-supported-clinical.

[16] https://www.nmpa.gov.cn/yaowen/ypjgyw/20201225204130191.html.

[17] H.S. Walter, S.A. Rule, M.J.S. Dyer, L. Karlin, C. Jones, B. Cazin, P. Quittet, N. Shah, C.V. Hutchinson, H. Honda, K. Duffy, J. Birkett, V. Jamieson, N. Courtenay-Luck, T. Yoshizawa, J. Sharpe, T. Ohno, S. Abe, A. Nishimura, G. Cartron, F. Morschhauser, C. Fegan, G. Salles, A phase 1 clinical trial of the selective BTK inhibitor ONO/GS-4059 in relapsed and refractory mature B-cell malignancies, Blood 127 (2016) 411–419, https://doi.org/10.1182/blood-2015-08-664086.

[18] R. Gabizon, N. London, A fast and clean BTK inhibitor, J. Med. Chem. 63 (2020) 5100–5101, https://doi.org/10.1021/acs.jmedchem.0c00597.

[19] W. Kawahata, T. Asami, T. Irie, M. Sawa, Design and synthesis of novel pyrimidine analogs as highly selective, non-covalent BTK inhibitors, Bioorg. Med. Chem. Lett. 28 (2018) 145–151, https://doi.org/10.1016/j.bmcl.2017.11.037.

[20] W.B. Young, J. Barbosa, P. Blomgren, M.C. Bremer, J.J. Crawford, D. Dambach, C. Eigenbrot, S. Gallion, A.R. Johnson, J.E. Kropf, S.H. Lee, L. Liu, J.W. Lubach, J. Macaluso, P. Maciejewski, S.A. Mitchell, D.F. Ortwine, J. Di Paolo, K. Reif, H. Scheerens, A. Schmitt, X. Wang, H. Wong, J.M. Xiong, J. Xu, C. Yu, Z. Zhao, K. S. Currie, Discovery of highly potent and selective Bruton's tyrosine kinase inhibitors: pyridazinone analogs with improved metabolic stability, Bioorg. Med. Chem. Lett. 26 (2016) 575–579, https://doi.org/10.1016/j.bmcl.2015.11.076.

[21] W.B. Young, J. Barbosa, P. Blomgren, M.C. Bremer, J.J. Crawford, D. Dambach, S. Gallion, S.G. Hymowitz, J.E. Kropf, S.H. Lee, L. Liu, J.W. Lubach, J. Macaluso, P. Maciejewski, B. Maurer, S.A. Mitchell, D.F. Ortwine, J. Di Paolo, K. Reif, H. Scheerens, A. Schmitt, C.G. Sowell, X. Wang, H. Wong, J.M. Xiong, J. Xu, Z. Zhao, K.S. Currie, Potent and selective Bruton's tyrosine kinase inhibitors: discovery of GDC-0834, Bioorg. Med. Chem. Lett. 25 (2015) 1333–1337, https://doi.org/10.1016/j.bmcl.2015.01.032.

[22] F.S. Ran, Y. Liu, M.X. Liu, D.G. Zhang, P. Wang, J.Z. Dong, W.D. Tang, G.S. Zhao, Discovery of pyrazolopyrimidine derivatives as potent BTK inhibitors with effective anticancer activity in MCL, Bioorg. Chem. 89 (2019), 102943, https://doi.org/10.1016/j.bioorg.2019.102943.

[23] I. Muqbil, M. Chaker, A. Aboukameel, R.M. Mohammad, A.S. Azmi, R. Ramchandren, Pre-clinical anti-tumor activity of Bruton's Tyrosine Kinase inhibitor in Hodgkin's Lymphoma cellular and subcutaneous tumor model, Heliyon 5 (2019), e02290, https://doi.org/10.1016/j.heliyon.2019.e02290.

[24] J. Wang, X.Y. Liu, Y.Z. Hong, S.T. Wang, P. Chen, A.H. Gu, X.Y. Guo, P. Zhao, Ibrutinib, a Bruton's tyrosine kinase inhibitor, exhibits antitumoral activity and induces autophagy in glioblastoma, J. Exp. Clin. Canc. Res. 36 (2017) 96, https://doi.org/10.1186/s13046-017-0549-6.

[25] J.Q. Qian, Z.Y. Xu, C. Meng, J. Liu, P.L. Hsu, Y.Y. Li, W.Z. Zhu, Y.M. Yang, S. L. Morris-Natschke, K.H. Lee, Y.N. Zhang, Y. Ling, Design and synthesis of benzylidenecyclohexenones as TrxR inhibitors displaying high anticancer activity and inducing ROS, apoptosis, and autophagy, Eur. J. Med. Chem. 204 (2020), 112610, https://doi.org/10.1016/j.ejmech.2020.112610.

[26] F. Honda, H. Kano, H. Kanegane, S. Nonoyama, E.S. Kim, S.K. Lee, M. Takagi, S. Mizutani, T. Morio, The kinase Btk negatively regulates the production of reactive oxygen species and stimulation-induced apoptosis in human neutrophils, Nat. Immunol. 13 (2012) 369–378, https://doi.org/10.1038/ni.2234.

[27] G. Galicia-Vazquez, S. Smith, R. Aloyz, Del11q-positive CLL lymphocytes exhibit altered glutamine metabolism and differential response to GLS1 and glucose metabolism inhibition, Blood Cancer J. 8 (2018) 13, https://doi.org/10.1038/s41408-017-0039-2.

[28] D. Khurana, L.N. Arneson, R.A. Schoon, C.J. Dick, P.J. Leibson, Differential regulation of human NK cell-mediated cytotoxicity by the tyrosine kinase Itk, J. Immunol. 178 (2007) 3575–3582, https://doi.org/10.4049/jimmunol.178.6.3575.

[29] F. Da Roit, P.J. Engelberts, R.P. Taylor, E.C.W. Breij, G. Gritti, A. Rambaldi, M. Introna, P.W.H.I. Parren, F.J. Beurskens, J. Golay, Ibrutinib interferes with the cell-mediated anti-tumor activities of therapeutic CD20 antibodies: implications for combination therapy, Haematologica 100 (2015) 77–86, https://doi.org/10.3324/haematol.2014.107011.

[30] F.S. Ran, Y. Liu, D.G. Zhang, M.X. Liu, G.S. Zhao, Discovery of novel pyrazole derivatives as potential anticancer agents in MCL, Bioorg. Med. Chem. Lett. 29 (2019) 1060–1064, https://doi.org/10.1016/j.bmcl.2019.03.005.

[31] F.S. Ran, Y. Liu, S.P. Yu, K.W. Guo, W.D. Tang, X. Chen, G.S. Zhao, Design and synthesis of novel 1-substituted 3-(6-phenoxypyridin-3-yl)-1H-pyrazolo[3,4-d] pyrimidin-4-amine analogs as selective BTK inhibitors for the treatment of mantle cell lymphoma, Bioorg. Chem. 94 (2020), 103367, https://doi.org/10.1016/j.bioorg.2019.103367.